Supporting information for

Robust Oil-Fouling Resistance of Amorphous Cellulose Surface Underwater: A Wetting Study and Application

Xin Zhou,[†] *J.Justin Koh,*[†,§] *Chaobin He*[*,†,‡]

†Department of Materials Science and Engineering, National University of Singapore, 117574, Singapore

‡Institute of Materials Research and Engineering, A*STAR (Agency for Science, Technology, and Research), 2 Fusionopolis Way, Innovis, Singapore 138634, Singapore

§Singapore Institute of Manufacturing Technology, Agency for Science, Technology and Research (A*STAR), 73 Nanyang Drive, 637662, Singapore

Corresponding Author

*E-mail: msehc@nus.edu.sg.

1. Soybean oil dewetting underwater

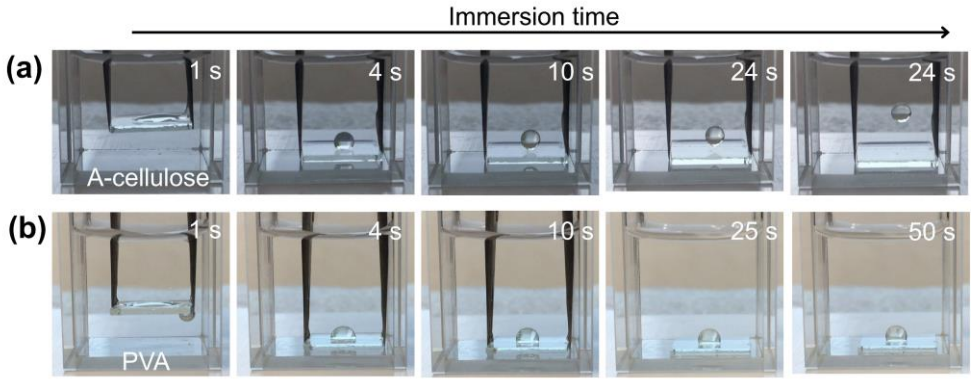

Figure S1. Consecutive still frames of the de-wetting of oil droplets (soybean oil, 20 μL) from a-cellulose and PVA surfaces underwater.

2. Contact angle data and calculations

Table S1. Surface tensions and interfacial tensions (mN/m) of the probe liquids

Liquid	γ^d	γ^p	γ^v	$\gamma_{o/w}{}^a$
Water	21.8	51.0	72.8	-
Methylene iodide (MI)	50.90	0.08	50.98	-
Hexadecane (HD)	27.6	0	27.6	46.70
Polydimethylsiloxane	21.0	0	21.0	42.49
Chloroform	25.9	1.6	27.5	31.60

[a] $\gamma_{o/w}$ denotes the interfacial tensions between water and oil phases, which were determined by Wilhelmy plate method.

2.1 Solid/air interfaces

The surface tensions of solid surfaces were calculated by Geometric-Mean equation from Young's equation:

$$(1+\cos\theta_l)\gamma_l = 2\left(\sqrt{\gamma_l^d\gamma_s^d}+\sqrt{\gamma_l^p\gamma_s^p}\right) \quad \text{S1}$$

the surface tension components of the substrate can be obtained by measuring the contact angles of two known surface tension testing liquids (water and methylene iodide). The results are tabulated in Table S3.

Table S2. Static and dynamic contact angles θ (°) of the probe liquids for different surfaces

Substrates	θ_{water} [a]	θ_{MI} [a]	θ^{A}_{PDMS} [b]	θ^{R}_{PDMS} [b]	θ^{A}_{water} [b]	θ^{R}_{water} [b]	$\Delta\theta_{water}$ [c]
CA	64.5±2.1	48.0±1.3	18.0±0.4	0	64.8±0.8	25.9±1.4	38.9
PVA	57.7±1.1	45.6±1.1	17.6±0.7	0	77.9±1.5	20.0±0.2	57.9
Cellulose	16.7±1.2	40.0±2.6	18.0±0.6	0	29.0±0.8	3.5±1.2	25.5
Glass	16.0±1.6	52.0±1.5	17.8±1.6	0	25.6±1.1	3.3±1.3	22.3

[a] Determined by sessile drop method and the volume of probe liquid is 2 μL. [b] Determined by Wilhelmy plate method. θ^{A} and θ^{R} denote the advancing angle and receding angle, respectively. [c] $\Delta\theta$ represents contact angle hysteresis (θ_A-θ_R).

2.2 Calculation of the theoretical oil contact angle in water

Table S3. Surface tensions and interfacial tensions (mN/m) of surfaces

Substrates	Surface tension γ [a]			$\gamma_{s/w}$ [b]	$\gamma_{s/o}$ [b]
	γ^{d}	γ^{p}	γ^{v}		
CA	34.0	12.0	46.0	14.7	25.3
PVA	35.0	15.5	50.5	11.6	29.8
A-cellulose	37.4	35.3	72.7	3.0	52.0
Glass	30.5	40.7	71.2	1.2	50.5

[a]Determined with contact angles of water and methylene iodide droplets by Geometric-Mean Method. [b]The interfacial tensions between solid and liquids were estimated with contact angles of water and PDMS in air by Young's equation.

According to Young's equation, the static contact angle is a result of a mechanical equilibrium among the three surface tensions at the contact line, therefore, the contact angles

of oil underwater can be expressed as below:

$$\gamma_{s/w} - \gamma_{s/o} = \gamma_{o/w} \cos\theta_{o/w} \quad \text{S2}$$

where $\gamma_{s/w}$ is the solid/water interfacial tension, $\gamma_{s/o}$ the solid/oil interfacial tension, and $\gamma_{o/w}$ the oil/water interfacial tension.

Then, one can obtain:

$$\theta_{o/w}^{cal} = \cos^{-1}\frac{\gamma_{s/w}-\gamma_{s/o}}{\gamma_{o/w}} \quad \text{S3}$$

which is the theoretical oil contact angle underwater on a flat surface. In this work, PDMS is chosen as the model oil phase due to its suitable density (0.966 g/mL) as compared with that of water (0.997 g/mL). $\gamma_{o/w}$ is 42.49 mN/m determined by Wilhelmy plate method. The values of $\gamma_{s/w}$ and $\gamma_{s/o}$ are listed in Table S3. $\gamma_{s/w}$ is estimated from the static water contact angle θ_{water}. $\gamma_{s/o}$ is estimated from the PDMS contact angle which is assumed to be 9° ($\theta_{PDMS} = \frac{\theta_{PMDS}^{A}+\theta_{PDMS}^{R}}{2}$) for all the surfaces.

3. Surface morphology

AFM images of PVA and glass show a quite smooth surface without any structural features. In contrast, the CA surface shows a spherically shaped structure feature in the nanometer scale. This could be attributed to the CA aggregation in acetone. After the hydrolysis reaction, the resulting cellulose surface displays identical features compared with the CA surface. The cellulose surface becomes smoother due to the hydrolysis and rinsing treatment.

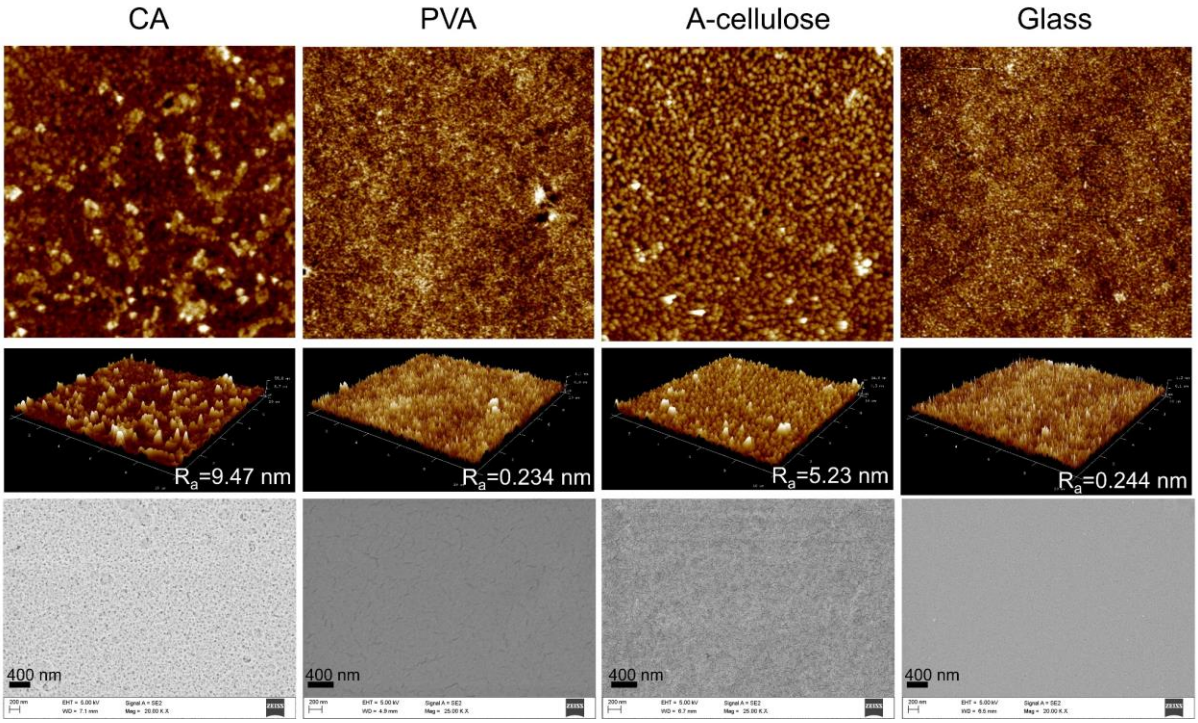

Figure S2. AFM tapping mode height images of the surfaces used in this study (the first two rows), all images were recorded with an area of 100 μm^2. The last row shows the SEM images of corresponding surfaces.

4. The modified Wilhelmy plate method

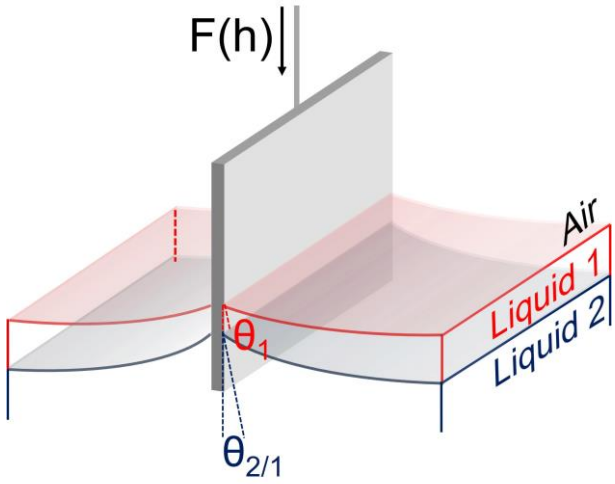

Figure S3. Schematic diagram of a Wilhelmy plate with double liquid lamellas

The Wilhelmy plate method is modified by using the double-liquids systems to elucidate the

dynamic wetting behavior of the substrates at interfaces, as schematically illustrated in Figure S3. The double-side coated plate (rectangle, 22×22×0.14 mm) is slowly immersed to a depth under the interfaces between liquid 1 and liquid 2, and then completely withdrew from the liquid reservoir. The force is detected as a function of position during the advancing and receding process. Since the balance with the plate is tared before contacting with liquid 1, the measured force is given by the equation:

$$F(h) = P\gamma_1 \cos\theta_1 + P\gamma_{12} \cos\theta_{2/1} + F_b(h) \quad \text{S4}$$

where F(h) is the force measured by the tensiometer, h the immersion depth, P the wetted perimeter of the plate, γ_1 the surface tension of the probe liquid 1, γ_{12} the interfacial tension between liquid 1 and liquid 2, θ_1 the liquid 1/solid/air contact angle, $\theta_{2/1}$ the liquid 2/solid/liquid 1 contact angle, F_b the buoyancy force. The physical meanings of the three terms on the right side of Eq. S4 are the wetting/dewetting force of liquid 1, wetting/dewetting force of the liquid 1/liquid 2 interface and the buoyancy force, respectively. Due to the small density difference between liquid 1 and 2, the buoyancy force can be approximated by a linear function:

$$F_b(h) = Ch \quad \text{S5}$$

where the slope C can be determined by regression of the linear region of Wilhelmy curves. Using the experimentally determined parameters above, the dynamic contact angles of the liquid 2 under liquid 1 can be computed as below:

$$\theta_{2/1} = \cos^{-1}\left(\frac{F(h) - P\gamma_1 \cos\theta_1 - Ch}{P\gamma_{12}}\right) \quad \text{S6}$$

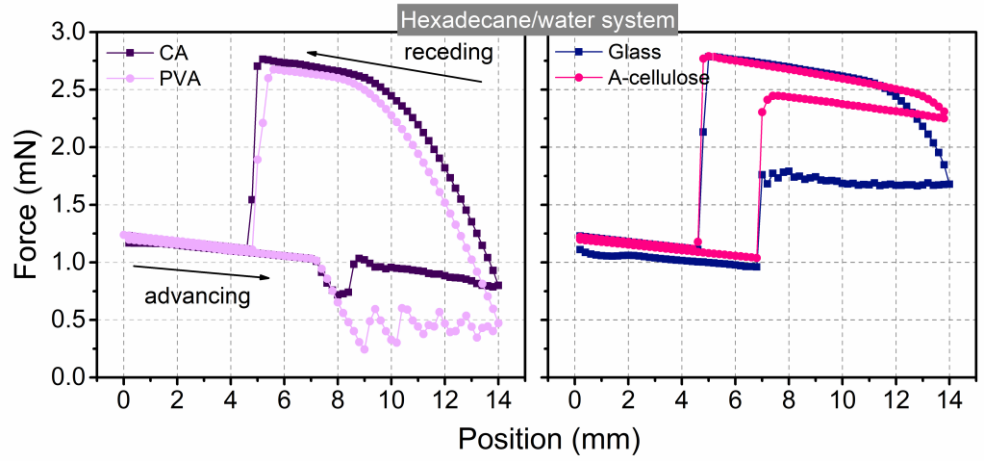

Figure S4. The plots display the vertical force F as a function of immersion depth h while the plate moves into the liquid reservoir of layered HD/water.

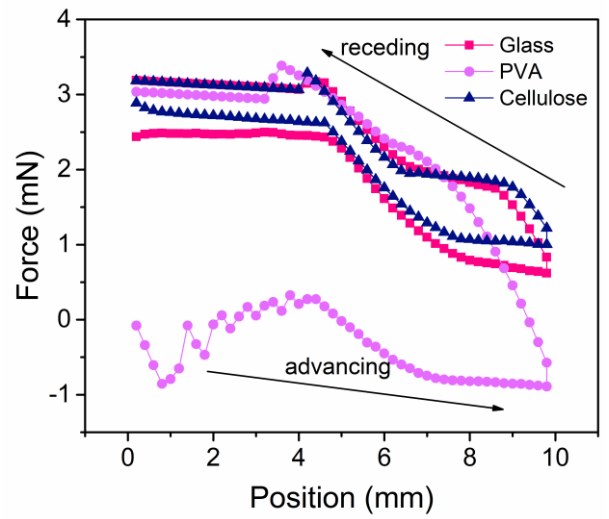

Figure S5. The plots display the vertical force F as a function of immersion depth h while the plate moves through the liquid reservoir of layered water/chloroform.

5. Structure of a-cellulose

The structure of amorphous cellulose was confirmed by XRD and polarized optical microscopy. As can be seen from Fig.S6 (a), there are no significant differences between the XRD profiles of the samples. All the diffraction profiles are very diffuse, indicating the lack of crystallinity. Similarly, the 2D SAXS data in Fig.S6 (b) shows the absence of long-range order.

Observations made using the polarizing microscope (POM) also indicates the inability of the a-cellulose film to polarized light, in contrast to the crystalline cellulose fiber (Fig.S6 c). These results suggest that the prepared a-cellulose film is a homogenous structure without any detectable long-range order. The supramolecular structure of amorphous cellulose could be described as a homogenous network where the polymer chains are held together by isotropically distributed hydrogen bonds. There may also exist hydrogen bond rich and hydrogen bond poor regions according to the previous study.[1]

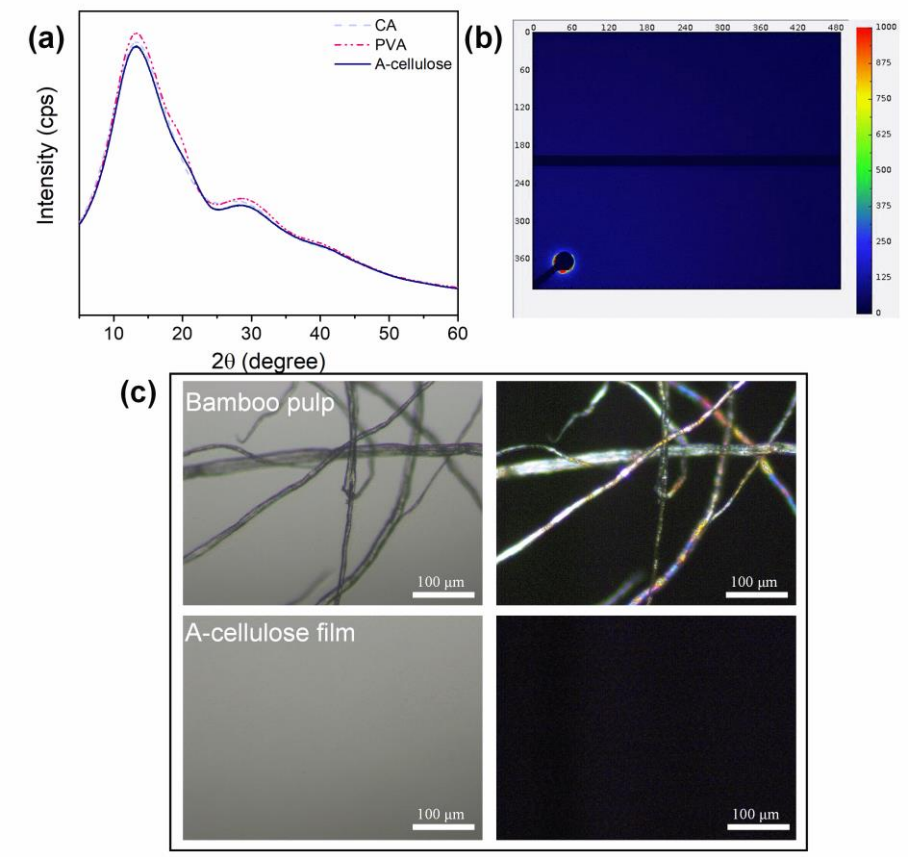

Figure S6. (a) Small incidence angle X-ray diffraction profiles of the polymer films. (b) The small-angle X-ray scattering (SAXS) pattern of the a-cellulose film. (c) Optical microscopy images of natural bamboo cellulose fiber and a-cellulose film and their polarized optical microscopy (POM) images.

6. Oil/water separation

Measurement of membrane flux was performed by using the apparatus with an effective filtration area of 4.9 cm^2 at a constant liquid height. The membrane flux per unit applied pressure was determined by measuring the volume of liquid permeated within 1 min via $J=Q/Atp$ where Q is the volume of permeate (L); A is effective filtration area (m^2); t is filtration time (h); p is the hydrostatic pressure.

The benchtop dead-end microfiltration apparatus shown in Figure 5a (manuscript) was used to evaluate the separation efficiency and long-term performance of the membrane. Free oil/water mixture (10 mL oil/40 mL seawater) was poured into the upper tube and then the rejected oil in the upper tube was collected and measured by a volume cylinder. The separation efficiency was calculated by the equation:

$$\mathrm{E} = \frac{V_C}{V_i} \times 100\%$$

where V_c is the volume of collected oil after separation and V_i is the initial volume of oil before mixing with water.

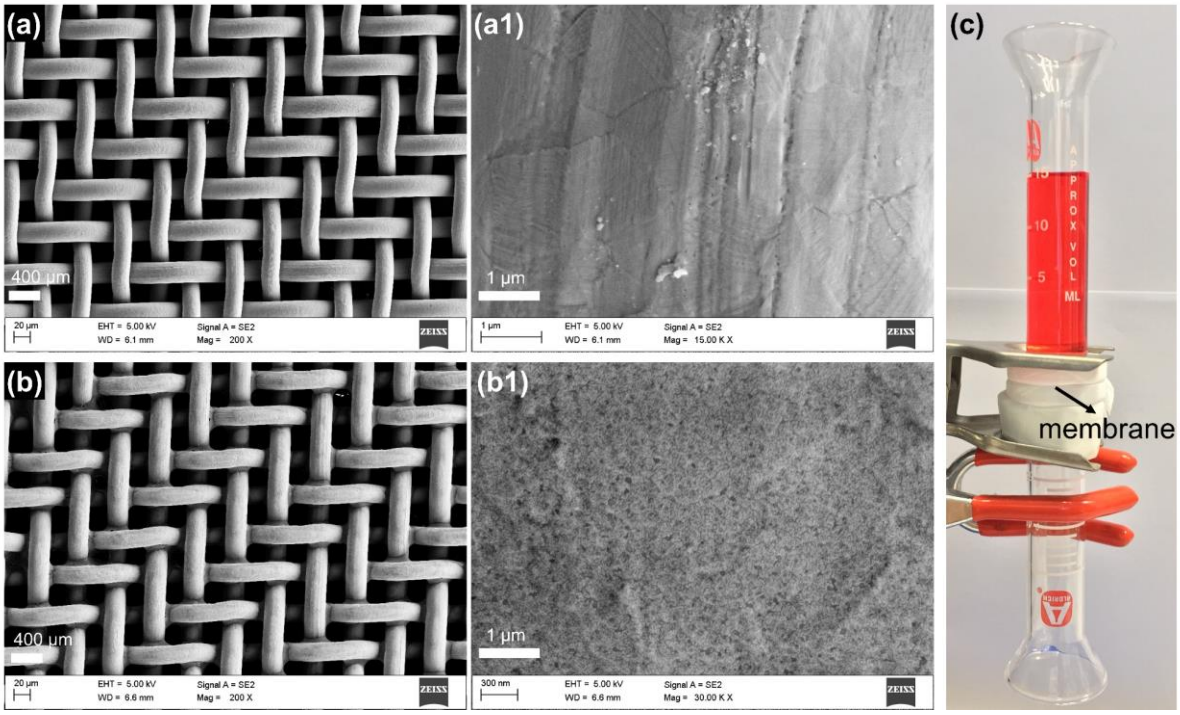

Figure S7. SEM images of (a) the O_2 plasma treated stainless steel mesh and (b) a-cellulose coated stainless-steel mesh (membrane). (a1) and (b1) show the corresponding high magnification views of metal wire surfaces. (c) separation apparatus with a mineral oil column above the membrane prewetted by seawater. No leaking oil was found in the lower tube after 10 min.

4 References

1. Kondo, T.; Sawatari, C., A Fourier transform infra-red spectroscopic analysis of the character of hydrogen bonds in amorphous cellulose. *Polymer* **1996,** *37* (3), 393-399.